

## RESEARCH ARTICLE

# Knockdown of circHIPK3 promotes the osteogenic differentiation of human bone marrow mesenchymal stem cells through activating the autophagy flux

Ziyao Zhuang<sup>1,2</sup>  | Chanyuan Jin<sup>2,3</sup>  | Xiaobei Li<sup>1,2</sup>  | Yineng Han<sup>1,2</sup>  |  
 Qiaolin Yang<sup>1,2</sup>  | Yiping Huang<sup>1,2</sup>  | Yunfei Zheng<sup>1,2</sup>  | Weiran Li<sup>1,2</sup> 

<sup>1</sup>Department of Orthodontics, Peking University School and Hospital of Stomatology, Beijing, China

<sup>2</sup>National Center of Stomatology, National Clinical Research Center for Oral Diseases, National Engineering Laboratory for Digital and Material Technology of Stomatology, Beijing, China

<sup>3</sup>Second Clinical Division, Peking University School and Hospital of Stomatology, Beijing, China

## Correspondence

Yunfei Zheng and Weiran Li,  
 Department of Orthodontics, Peking University School and Hospital of Stomatology, 22 Zhongguancun Avenue South, Haidian District, Beijing 100081, China.  
 Email: [yunfei\\_zheng@bjmu.edu.cn](mailto:yunfei_zheng@bjmu.edu.cn) and [weiranli@bjmu.edu.cn](mailto:weiranli@bjmu.edu.cn)

## Funding information

National Natural Science Foundation of China (NSFC), Grant/Award Number: 82071142 and 82071119

## Abstract

Many circular RNAs (circRNAs) involved in the osteogenesis of human bone marrow mesenchymal stem cells (hBMSCs) have recently been discovered. The role of circHIPK3 in osteogenesis has yet to be determined. Cell transfection was conducted using small-interfering RNAs (siRNAs). Expression of osteogenic markers were detected by quantitative reverse transcription-polymerase chain reaction, western blotting analysis, and immunofluorescence staining. Ectopic bone formation models in nude mice were used to examine the bone formation ability in vivo. The autophagy flux was examined via western blotting analysis, immunofluorescence staining and transmission electron microscopy analysis. RNA immunoprecipitation (RIP) analysis was carried out to analyze the binding between human antigen R (HUR) and circHIPK3 or autophagy-related 16-like 1 (ATG16L1). Actinomycin D was used to determine the mRNA stability. Our results demonstrated that silencing circHIPK3 promoted the osteogenesis of hBMSCs while silencing the linear mHIPK3 did not affect osteogenic differentiation, both in vivo and in vitro. Moreover, we found that knockdown of circHIPK3 activated autophagy flux. Activation of autophagy enhanced the osteogenesis of hBMSCs and inhibition of autophagy reduced the osteogenesis through using autophagy regulators chloroquine and rapamycin. We also discovered that circHIPK3 and ATG16L1 both bound to HUR. Knockdown of circHIPK3 released the binding sites of HUR to ATG16L1, which stabilized the mRNA expression of ATG16L1, resulting in the upregulation of ATG16L1 and autophagy activation. CircHIPK3 functions as an osteogenesis and autophagy regulator and has the potential for clinical application in the future.

## KEYWORDS

autophagy, BMSCs, circHIPK3, human antigen R (HUR), osteogenesis

**Abbreviations:** ALP, alkaline phosphatase; ARS, alizarin red S; ATGs, autophagy-related genes; ATG16L1, autophagy related 16-like 1; circRNAs, circular RNAs; CQ, chloroquine; ELAVL1/HUR, ELAV-like RNA binding protein 1/human antigen R; GAPDH, glyceraldehyde 3-phosphate dehydrogenase; GM, growth medium; hBMSCs, human bone marrow mesenchymal stem cells; H&E, hematoxylin and eosin; lncRNAs, long non-coding RNAs; OCN, osteocalcin; OM, osteogenic medium; PBS, phosphate buffer saline; qRT-PCR, quantitative reverse transcription-polymerase chain reaction; Rapa, rapamycin; RIP, RNA Immunoprecipitation; RUNX2, RUNX family transcription factor 2; SD, standard deviation; siRNAs, small interfering RNAs; TEM, transmission electron microscopy.

## 1 | INTRODUCTION

Mesenchymal stem cells are able to differentiate into osteoblasts and are potential candidates for the treatment of bone defects. Bone marrow mesenchymal stem cells (BMSCs) are the most commonly studied MSCs with many preclinical and clinical studies of BMSC-based treatments for bone restoration.<sup>1–3</sup> In some studies, BMSCs were genetically engineered to express specific genes or differentiate into specific cell lines before implantation to improve their osteogenic ability.<sup>4,5</sup>

Circular RNA (circRNA) was named after its ring-like structure. Unlike linear RNA, it is a covalently closed loop without a 5' cap and poly A tail.<sup>6</sup> It has multiple biological functions. Some can serve as miRNAs or protein sponges, where circRNAs bind to miRNAs or proteins and then suppress their effects.<sup>6,7</sup> Some circRNAs can affect gene transcription and others are translated into proteins or peptides.<sup>8–10</sup> Numerous studies have proven that circRNAs are involved in the osteogenic differentiation of BMSCs. CircHIPK3 (circRNA ID: hsa\_circ\_0000284) is formed by the second exon of HIPK3. The flanking introns of HIPK3 Exon2 showed highly complementary Alu repeats which could pair and then trigger direct circularization.<sup>11</sup> CircHIPK3 has been widely reported to act as a sponge for different miRNAs to block them from binding to their target mRNAs and then regulate gene expression in the post-transcriptional.<sup>11–13</sup> Its other potential roles, such as protein sponge or peptide translator, still wait to be explored. CircHIPK3 has been studied mostly in cancer. It was involved in the occurrence and development of various cancers such as lung cancer,<sup>14</sup> colorectal cancer,<sup>12</sup> and bladder cancer.<sup>15</sup> CircHIPK3 affected tumor via regulating different cellular processes such as proliferation, angiogenesis, and metastasis.<sup>16</sup> However, few has focused on its relationship with osteogenesis. In a previous study, we found that circHIPK3 was differentially expressed during the osteogenesis of periodontal ligament stem cells in the RNA sequencing results.<sup>17</sup> We wondered if it played a role in the osteogenic differentiation of BMSCs.

Autophagy is a major type of cellular activity that is very sensitive to environmental changes such as starvation and other stresses. It functions in the degradation and reuse of cytoplasmic materials, and can be thought of as an “intracellular recycling system.”<sup>18</sup> Autophagy is involved in several signaling pathways related to cell differentiation: Wnt/ $\beta$ -catenin, Notch, Nrf2/keap1 signaling, and so forth.<sup>19</sup> The relationship between autophagy and osteogenic differentiation has been studied and debated in numerous studies. Many studies showed that the activation of autophagy promoted osteogenesis in various cell types, such as gingival MSCs,<sup>20</sup> ligamentum fibroblasts,<sup>21</sup> BMSCs,<sup>22–24</sup> and dental pulp stem cells.<sup>25</sup> Conversely, inducing autophagy can suppress osteogenesis in dental follicle cells,<sup>26</sup> vascular smooth muscle cells,<sup>27,28</sup> and MC3T3-E1 cells.<sup>29</sup> Autophagy-related genes (ATGs) are a

large family and more than 40 members are involved in autophagy regulation.<sup>30</sup> Autophagy-related 16-like 1 (ATG16L1) is a core autophagy-related protein that interacts with ATG5 and ATG12 to form a large multimeric complex, resulting in LC3B lipidation and the activation of autophagy flux.<sup>20</sup> LC3B is a ubiquitin-like protein with two forms: non-lipidated LC3B-I and lipidated LC3B-II. Accumulation of LC3B-II is a sensitive marker of autophagy activation. Another autophagy marker is SQSTM1/P62, whose degradation marks the activation of autophagy.<sup>31</sup> In the present study, P62 and LC3B were chosen to detect autophagy activity.

ELAV-like RNA-binding protein 1/human antigen R (ELAVL1/HUR) is a widely studied RNA-binding protein. HUR interacts with non-coding RNAs, including circRNAs, miRNAs and long non-coding RNAs (lncRNAs). For instance, a new lncRNA highly expressed in gallbladder cancer was found to stabilize itself through binding to HUR, thus promoting the progression of gallbladder cancer.<sup>32</sup> CircAGO2 interacted with HUR and facilitated its repression on AGO2/miRNA-mediated gene silencing and promoted tumorigenesis and aggressiveness.<sup>33</sup>

Here, we examined the role of circHIPK3 in osteogenesis both in vitro and in vivo. Then we determined its role in the autophagy of human BMSCs (hBMSCs) and explored the relationship between these two biological behaviors.

## 2 | MATERIALS AND METHODS

### 2.1 | Cell culture and treatment

Human BMSCs were purchased from ScienCell company (Carlsbad, CA, USA). Cells were cultured in growth medium (GM) consisting of MEM alpha basic medium supplemented with 1% antibiotics and 10% fetal bovine serum. Osteogenesis was induced by culturing cells in the osteogenic medium (OM) consisting of 100 nM dexamethasone, 0.2 mM ascorbic acid, and 10 mM  $\beta$ -glycerophosphate added to standard GM. Adipogenesis was induced by culturing cells in GM supplemented with 10  $\mu$ g/ml insulin, 100 nM dexamethasone, 0.5 mM 3-isobutyl-1-methylxanthine, and 200  $\mu$ M indomethacin. Cells were washed using phosphate buffer saline (PBS), and the medium was changed every 2–3 days.

### 2.2 | Transfection

Small-interfering RNAs (siRNAs) targeting circHIPK3 (si-circ-1 and si-circ-2), mHIPK3 (si-lin), HUR (si-HUR-1 and si-HUR-2) and the scramble control (si-NC) were purchased from Integrated Biotech Solutions Co. (Shanghai, China). The sequences are listed in Table S1. When the

degree of cell fusion reached 70%–80%, cells were transfected with siRNAs using Opti-MEM and Lipofectamine 3000 (Invitrogen) at 100 nM every 4 days according to the manufacturer's instructions.

### 2.3 | RNA isolation and quantitative reverse transcription-polymerase chain reaction (qRT-PCR) analysis

TRIzol (Thermo Fisher Scientific) was used to extract total RNAs from cells. The RNA concentration was measured on a NanoDrop 2000 Spectrophotometer (Thermo Fisher Scientific). Then cDNA was prepared using the PrimeScript RT Reagent Kit (Takara, Tokyo, Japan). qRT-PCR analysis was performed using SYBR Green Master Mix (Roche Applied Science, Mannheim, Germany) on the 7500 real-time PCR System (Applied Biosystems, Foster City, CA, USA). Relative quantification of gene expression was calculated using the  $2^{-\Delta\Delta CT}$  method. Glyceraldehyde 3-phosphate dehydrogenase (GAPDH) was used for normalization. Primers sequences used are listed in Table S1.

### 2.4 | Alkaline phosphatase (ALP) staining and quantification

After 7 days of osteogenic induction, cells were fixed in 4% paraformaldehyde for 15 min and washed using distilled water for three times. ALP staining was performed using the BCIP/NBT Alkaline Phosphatase Color Development Kit (Beyotime, Shanghai, China). ALP activity was analyzed as described previously.<sup>34</sup> It was evaluated with the ALP Activity Kit (Biovision, Milpitas, CA) and normalized to the total protein contents.

### 2.5 | Alizarin red S (ARS) staining and quantification

After osteogenic induction for 14 days, cells were fixed in 4% paraformaldehyde for 15 min. Distilled water was used to wash the cells three times after fixation. ARS staining was performed using 1% Alizarin red S dye (Sigma-Aldrich; Merck KGaA) for 20 min. The staining of hBMSCs was solubilized by cetylpyridinium chloride and quantified by a spectrophotometer at 570 nm as described previously.<sup>34</sup>

### 2.6 | Oil red O staining

Oil red O staining was carried out as described previously.<sup>35</sup> Cells were fixed in 4% paraformaldehyde for

15 min. The cells were then rinsed with 60% isopropanol. Oil red O (0.3%, Sigma-Aldrich) was then added and incubated for 15 min. After staining, distilled water was used to wash the cells for three times and the staining was visualized by light microscopy. For quantitation, Oil red O was eluted by 100% isopropanol and quantified by spectrophotometric absorbance at 520 nm against a blank (100% isopropanol).

### 2.7 | Immunofluorescence staining

When the degree of cell fusion reached approximately 70%, cells were fixed in 4% paraformaldehyde for 15 min and permeabilized by 1% Triton X-100 for 10 min. After being washed with PBS for three times, cells were blocked in 5% goat serum (Zhongshan Golden Bridge Biotechnology, Beijing, China) for 1 h. Then cells were incubated in the primary antibodies osteocalcin (OCN) and RUNX family transcription factor 2 (RUNX2) at 1:200 (Cat No. 23418-1-AP and 20700-1-AP; Abcam, Cambridge, UK) overnight and washed using PBS three times, for 5 min each time. Then cells were incubated in anti-rabbit secondary antibody at 1:200 (Zhongshan Golden Bridge Biotechnology, Beijing, China) for 1 h. Nuclei was stained using DAPI, and then the cells were observed and photographed using a confocal system for imaging (LSM 5 EXCITER, Carl Zeiss, Jena, Germany).

### 2.8 | Western blotting analysis

Proteins were extracted using a radioimmunoprecipitation assay (RIPA) lysis buffer which consisted of 50 mM Tris-HCl (pH 7.4), 150 mM NaCl, 1% NP-40, and 0.1% SDS. Samples were separated by SDS-PAGE and transferred into PVDF membranes (Millipore, Billerica, MA, USA), which then were blocked for 1 h with skim milk and incubated with primary antibodies against RUNX2 (Cat No. 20700-1-AP; Abcam), LC3B (Cat No. 12741; Cell Signaling Technology), P62 (Cat No. 5114; Cell Signaling Technology), HUR (Cat No. 11910-1-AP; Proteintech, Wuhan, China), PPAR $\gamma$  (Cat ET1702-57; HuaAn Biotechnology, Hangzhou, China), FABP4 (Cat ET1703-98; HuaAn Biotechnology), CD36 (Cat ET1701-24; HuaAn Biotechnology) and GAPDH (Cat No. HX1828; HuaxingBio Science, Beijing, China) at 4°C overnight. RUNX2, LC3B, P62, HUR, PPAR $\gamma$ , FABP4, and CD36 were diluted 1:1000. GAPDH was diluted 1:5000. After being washed with TBS containing Tween-20, the membranes were incubated with secondary antibodies (Cat No. 7076, 7074; 1:10000, Cell Signaling Technology) for 1 h at room temperature. Protein bands were visualized using the ECL Kit (CoWin Biotech). The intensity of protein band

was measured by Image J software and the fold change was listed under each protein band and normalized to GAPDH.

## 2.9 | Ectopic bone formation in vivo

The hBMSCs transfected with siRNAs were cultured in OM for 1 week before the experiments. Then,  $5 \times 10^6$  cells were resuspended and incubated with  $7 \times 5 \times 2$  mm Bio-Oss Collagen (Geistlich, GEWO GmbH, Baden-Baden, Germany) scaffolds for 1 h at  $37^\circ\text{C}$ . Then the cell–collagen complexes were implanted subcutaneously into the dorsal surface of 8-week-old BALB/c homozygous nude (nu/nu) male mice (6 mice per group), as described previously.<sup>36,37</sup> The mice were purchased from Charles River Laboratories (Beijing, China) and maintained under specific pathogen-free condition. The mice were randomized into four groups: si-NC-hBMSCs/Collagen group, si-circ-1-hBMSCs/Collagen group, si-circ-2-hBMSCs/Collagen group, and si-lin-hBMSCs/Collagen group. The mice were anesthetized with sodium pentobarbital (40 mg/kg, ip). After 8 weeks, all mice were killed by sodium pentobarbital overdose (100 mg/kg, i.p.). Implants were harvested and fixed in 4% paraformaldehyde, decalcified, and embedded in paraffin wax. Sections (5  $\mu\text{m}$ ) were cut, and H&E and Masson's trichrome staining and immunohistochemical analysis were performed to detect the expression level of OCN (Cat No. 23418-1-AP; Abcam). All animal experiments were approved by the Institutional Animal Care and Use Committee of the Peking University Health Science Center (LA2021078) and were performed according to the Institutional Animal Guidelines.

## 2.10 | RNA sequencing

Total RNA was extracted from all groups using TRIzol reagent (Thermo Fisher Scientific). cDNA libraries were constructed, and samples underwent paired-end sequencing using the NovaSeq6000 platform. Transcriptome sequencing data were mapped to the human genome (hg38) using TopHat2. We used HTseq to count the genes and calculate the reads per kilobase transcriptome per million mapped reads (RPKM) to evaluate the gene expression level. Differentially expressed genes were defined based on fold changes greater than or equal to 1.5 and a false discovery rate (FDR) of  $<0.05$ .

## 2.11 | Transmission electron microscopy (TEM)

BMSCs transfected with siRNAs were harvested and fixed in 2.5% glutaraldehyde at  $4^\circ\text{C}$  overnight ( $1 \times 10^6$  per

sample). Then, 1%  $\text{OsO}_4$  was used to further fix the samples. After stepwise dehydration in ascending acetone, the cells were embedded in epoxy-araldite resin following standard protocols. Afterwards, ultrathin sections were made and stained with uranyl acetate and lead citrate. The samples were examined with a transmission electron microscope (FEI Tecnai Spirit 120kV).

## 2.12 | RNA immunoprecipitation (RIP) analysis

The interaction probabilities between circHIPK3 and HUR were predicted using computational tools on the websites: <http://priddb.gdc.b.iastate.edu/RPISeq/results.php> and <https://circinteractome.nia.nih.gov/index.html>.<sup>38,39</sup> The sequences used for predicting the binding of circHIPK3 to HUR are shown in File S1. RNA immunoprecipitation (RIP) analysis was carried out using the Magna RIP™ RNA Binding Protein Immunoprecipitation Kit (BersinBio, Guangzhou, China) according to the manufacturer's instruction. Cells were lysed in cell lysis buffer and incubated with magnetic beads (Thermo Fisher Scientific) bound with anti-IgG and anti-HUR. Immunoprecipitated RNA complexes were purified with TRIzol reagent (Thermo Fisher). The expression of circHIPK3, HIPK3, and ATG16L1 mRNA was measured via qRT-PCR. The qRT-PCR analysis was carried out using IgG as the negative control and input for normalization.<sup>40</sup>

## 2.13 | RNA pull down assay

The circHIPK3, HIPK3, and control probes were purchased from DLMbiotech company (Wuhan, China). The RNA pull down assay was performed using the RNA pull down kit (BersinBio, Guangzhou, China) according to the manufacturer's instruction. Briefly,  $1 \times 10^7$  BMSCs were harvested and lysed. Subsequently, the probe-magnetic bead complex and cell extract were mixed and gently rotated for 2 h at  $25^\circ\text{C}$ . After washing with a magnetic rack, the protein bound to the beads was eluted and extracted for western blotting analysis.

## 2.14 | mRNA stability assay

To determine mRNA stability, cells were treated with actinomycin D (2.5  $\mu\text{g}/\text{ml}$ , Sigma) according to a previous study.<sup>41</sup> After silencing circHIPK3, HIPK3, HUR, and the control, actinomycin D was added to inhibit transcription at certain time points, and then cells were collected at the indicated time points. RNA was extracted and qRT-PCR was performed for the quantification of ATG16L1 mRNAs.

## 2.15 | Subcellular fractionation

Nuclear and cytoplasmic fractions of hBMSCs were isolated using the Nuclei Isolation Kit (Invent-biotech, Minnesota, USA). Briefly, cells were harvested and treated with the cytoplasm extraction buffer and 15s dynamic vortex. The mixtures were incubated on ice for 5 min and then centrifuged at top speed in a microcentrifuge at 4°C for 5 min. After centrifugation, RNA was extracted from both fractions using TRIzol and then reverse-transcribed into cDNA. The RNA expression was quantified by qRT-PCR. MALAT1, and GAPDH were used as fractionation indicators. The primers used are listed in Table S1.

## 2.16 | Statistical analysis

Statistical analyses were performed using SPSS version 16.0 (SPSS Inc., Chicago, IL, USA). The independent sample *t*-test was used to evaluate statistical differences between two groups, and one-way analysis of variance (ANOVA) was used to analyze the statistical significance when there were more than two groups. Results are presented as the mean  $\pm$  standard deviation (SD) of at least three independent experiments. We considered *p*-values  $<.05$  as statistically significant.

# 3 | RESULTS

## 3.1 | CircHIPK3 was upregulated during the osteogenic differentiation of hBMSCs

To elucidate the expression pattern of circHIPK3 in the osteogenesis of hBMSCs, we induced BMSCs to undergo 14 days of osteogenic differentiation and examined circHIPK3 expression. RNA expression of osteogenic markers ALP, RUNX2, and OCN was greatly increased during the osteogenesis (Figure 1A). The expression level of ALP, RUNX2, and OCN was the highest on the 10th day (more than 8-fold), 14th day (about 10-fold), and 7th day (more than 4-fold), respectively. CircHIPK3 was upregulated during the 14 days of osteogenic differentiation (Figure 1B). The change was statistically significant but not surprising, about twofold increase. We thought that it was due to the abundant expression of circHIPK3 in BMSCs. The protein level of RUNX2 also increased in 14 days, which was expected (Figure 1C). The mineralized nodules observed under a microscope were enlarged during the 14 days induction (Figure 1D). The staining and activity of ALP were increased more than 30-fold during the osteogenesis (Figure 1E). The intensity of alizarin red S (ARS) staining and quantification were also increased more than 40-fold

during the 14 days osteogenesis, indicating the successful osteogenic induction (Figure 1F).

## 3.2 | Knockdown of circHIPK3 promoted the osteogenic differentiation of hBMSCs in vitro

To examine the function of circHIPK3 in the osteogenic differentiation of hBMSCs, we used three siRNAs to knock down circHIPK3 and its linear mRNA (mHIPK3). The PCR results showed a high efficiency of silencing (more than 70%). The expression levels of some circRNAs and their linear mRNAs maybe interrelated in some cases. However, our results demonstrated that silencing circHIPK3 did not significantly affect the abundance of mHIPK3 produced by the host gene. At the same time, silencing mHIPK3 did not lead to significant decrease or increase of circHIPK3. So, the effects caused by circHIPK3 knockdown were independent of mHIPK3 (Figure 2A). Western blotting analysis showed that knockdown of circHIPK3 upregulated the protein level of RUNX2 about 2-fold while silencing HIPK3 had no change on day 7 of osteogenic induction (Figure 2B). ALP, RUNX2, and OCN were increased more than 6-fold, 2-fold, and 1.5-fold, respectively, after silencing circHIPK3 and remained unchanged after silencing HIPK3 on day 7 of osteogenesis (Figure 2C). ALP and ARS staining and quantification showed the same tendency: more than 1.5-fold increase of osteogenic activity was found in the circHIPK3 knockdown groups on days 7 and 14 of osteogenic induction compared to the mHIPK3 knockdown group and the control group (Figure 2D). Immunofluorescence staining analysis of RUNX2 and OCN protein expression showed an upregulation in the circHIPK3 knockdown groups on day 7 of osteogenesis and showed no change in the HIPK3 knockdown group compared to the control group (Figure 2E).

## 3.3 | Knockdown of circHIPK3 promoted bone formation in vivo

Ectopic bone formation was carried out to determine the role of circHIPK3 in osteogenesis in vivo (Figure 3A). Implants were harvested after 2 months. Hematoxylin and eosin (H&E) and Masson's trichrome staining results proved that the circHIPK3 knockdown groups (si-circ-1 and si-circ-2) resulted in more bone-like tissues compared to its control group (si-NC) and the HIPK3 silencing group (si-lin). Immunohistochemical analysis also indicated a higher expression level of OCN in the circHIPK3 knockdown groups compared to its control group (Figure 3B).

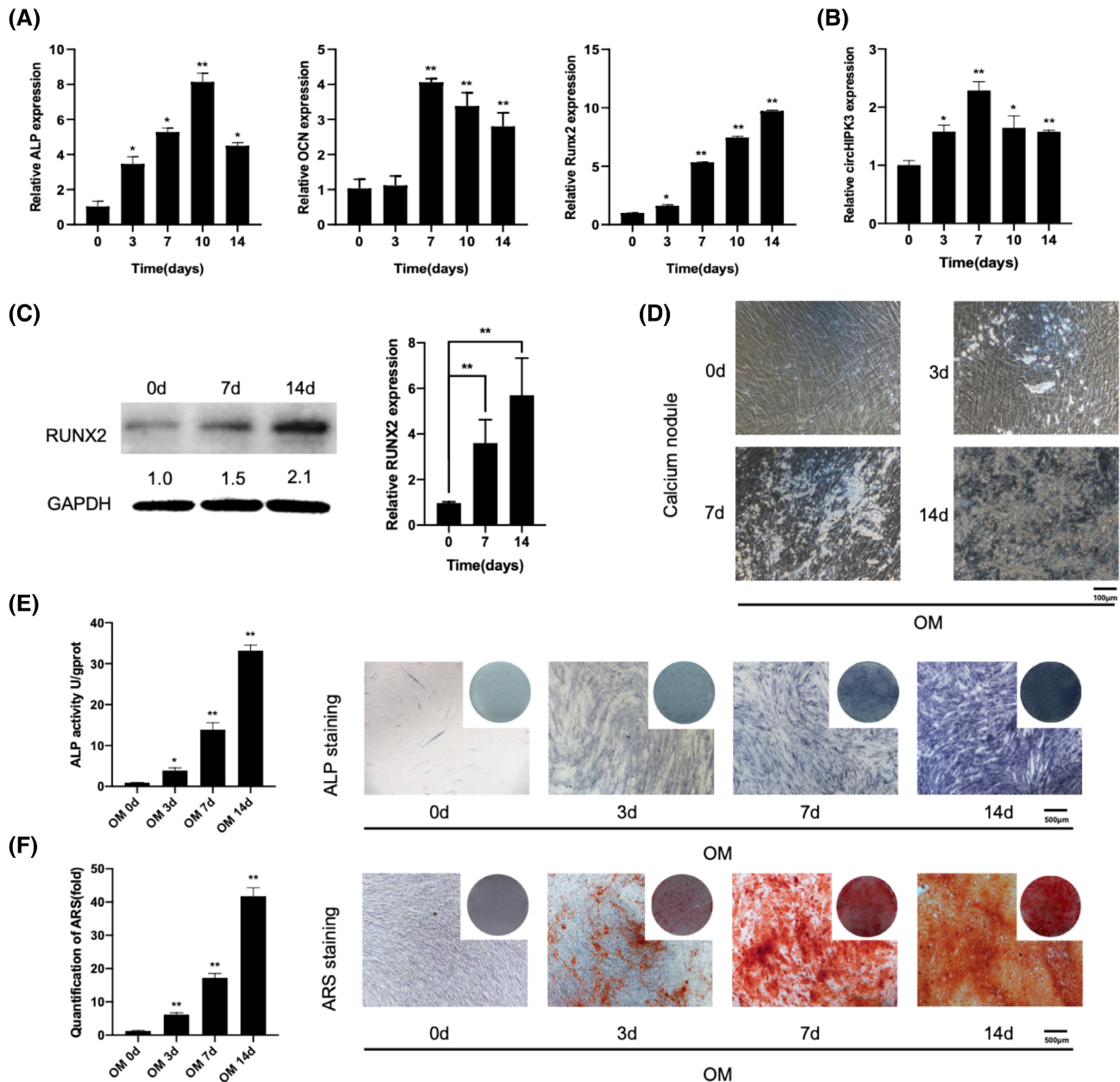


**FIGURE 1** CircHIPK3 was upregulated during the osteogenesis of hBMSCs. The expression level of osteo-related genes (A) and circHIPK3 (B) during the 14-day osteogenesis of hBMSCs was determined. (C) The protein level of RUNX2 was detected and at certain time points during osteogenesis. Quantification of band intensity was analyzed. (D) Mineralized nodules were observed using a microscope. ALP staining and quantification (E), and ARS staining and quantification (F) were performed (compared to the day 0 group; results are presented as the mean  $\pm$  SD; \* $p < .05$ ; \*\* $p < .01$ ).

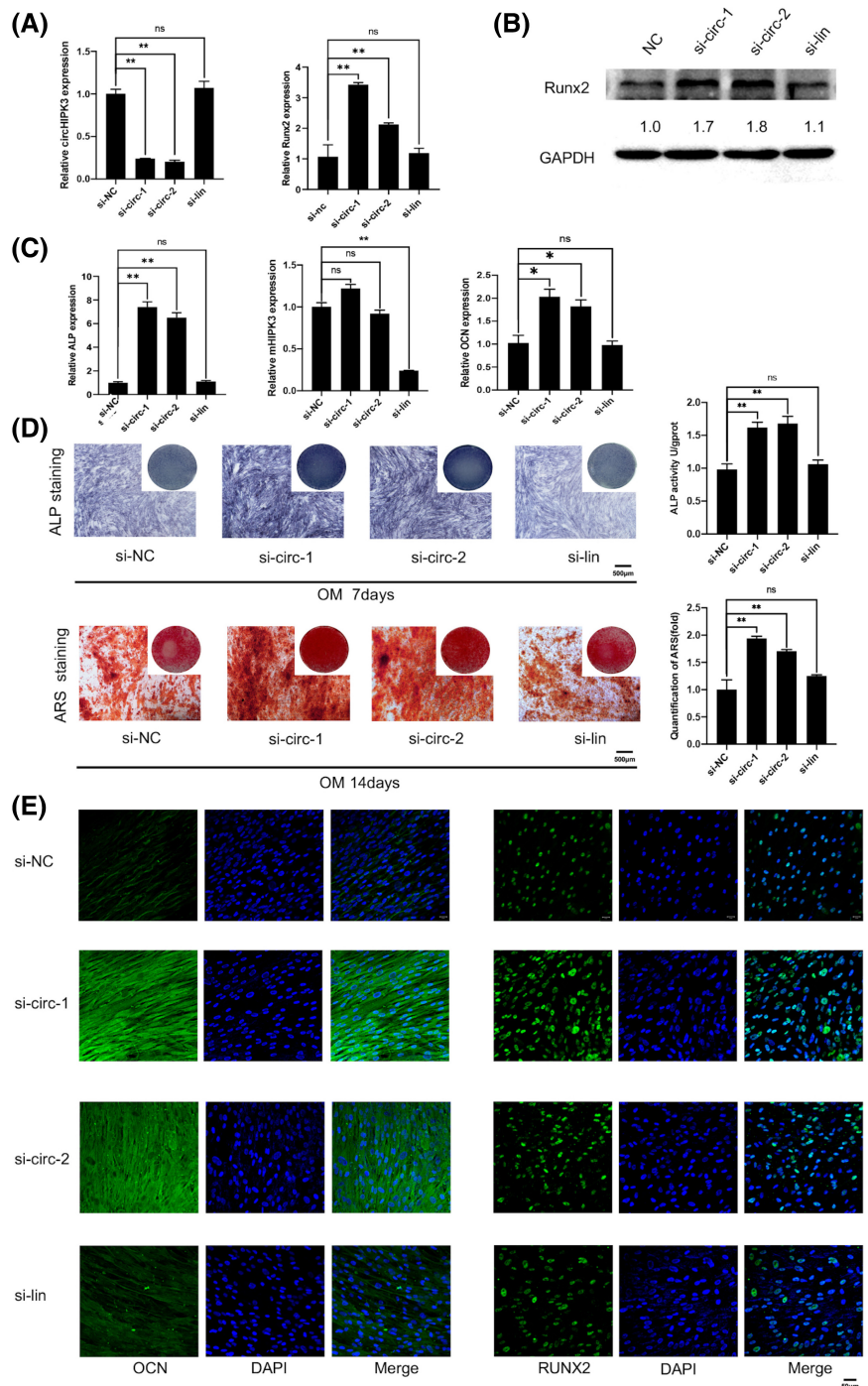
Knockdown of HIPK3 had no significant effect on bone formation in vivo.

### 3.4 | RNA sequencing results revealed circHIPK3 was involved in autophagy

To study the underlying mechanisms of circHIPK3 in the regulation of osteogenic differentiation, hBMSCs

transfected with siRNA targeting circHIPK3 and its negative control were collected and subjected to RNA sequencing. The transcriptome was analyzed using NovaSeq6000. Differential expression analysis and KEGG analysis were then conducted. The volcano plot revealed the genes that were differentially expressed following circHIPK3 knockdown (Figure 4A). Among these genes, 19 gene were significantly upregulated (FC  $> 1.5$ , FDR  $< 0.05$ ) and 65 genes were downregulated.

**FIGURE 2** Knockdown of circHIPK3 promoted the osteogenesis of hBMSCs in vitro. BMSCs were transfected with small-interfering RNAs targeting circHIPK3 (si-circ-1 and si-circ-2 group), HIPK3 (si-lin group), and negative control (si-NC group). (A) The efficiency of knockdown was examined using qRT-PCR. The protein level of RUNX2 (B) and the mRNA expressions of osteo-related genes (C) in the si-NC, si-circ-1, si-circ-2, and si-lin groups were detected after 7 days of osteogenic induction. (D) ALP staining and activity were performed on day 7 of osteogenesis. ARS staining and activity were performed on day 14 of osteogenic differentiation. (E) Immunofluorescence staining analysis of RUNX2 and OCN protein expression was conducted on day 7 of osteogenesis (compared to the si-NC group; results are presented as the mean  $\pm$  SD; \* $p < .05$ ; \*\* $p < .01$ ).



Among these genes, 36 genes were previously reported to be related with autophagy. The expression of five autophagy related genes (RICTOR, ISG15, IBTK, ATG16L1, and FAT4) was also validated by RT-PCR, and the results were consistent with the RNA sequencing (Figure S2). In addition, the KEGG pathway analysis indicated several pathways related to autophagy, such as the mTOR pathway and the MAPK pathway (Figure 4B). Therefore, we hypothesized that circHIPK3 affected BMSC autophagy and verified the role of circHIPK3 on autophagy.

### 3.5 | Silencing circHIPK3 activated autophagy flux

As mentioned above, we chose LC3B and P62 to detect autophagy flux. Western blotting analysis showed an increased conversion of LC3B-II into LC3B-I (more than 1.5-fold) and downregulated P62 (about 2-fold) upon circHIPK3 knockdown, suggesting that silencing circHIPK3 induced autophagy (Figure 5A). The upregulation of the conversion of LC3B-II into LC3B-I may be due to the accumulation of LC3B-II and may also be caused by

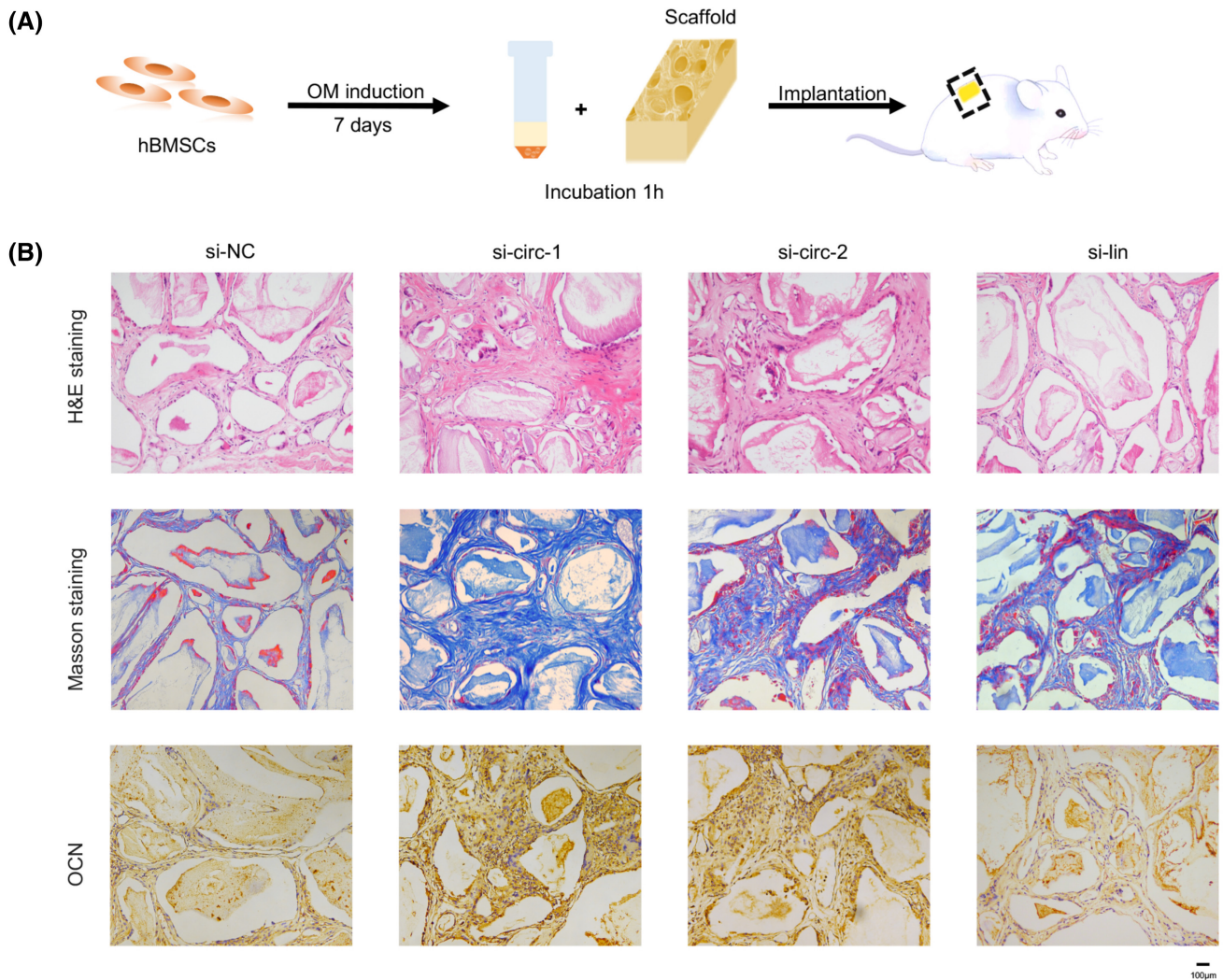


**FIGURE 3** Knockdown of circHIPK3 promoted bone formation in vivo. (A) The schematic diagram of the ectopic bone formation assay. (B) H&E and Masson's trichrome staining, immunohistochemical staining of OCN were carried out in the si-NC, si-circ-1, si-circ-2, and si-lin groups after 8 weeks of bone formation.

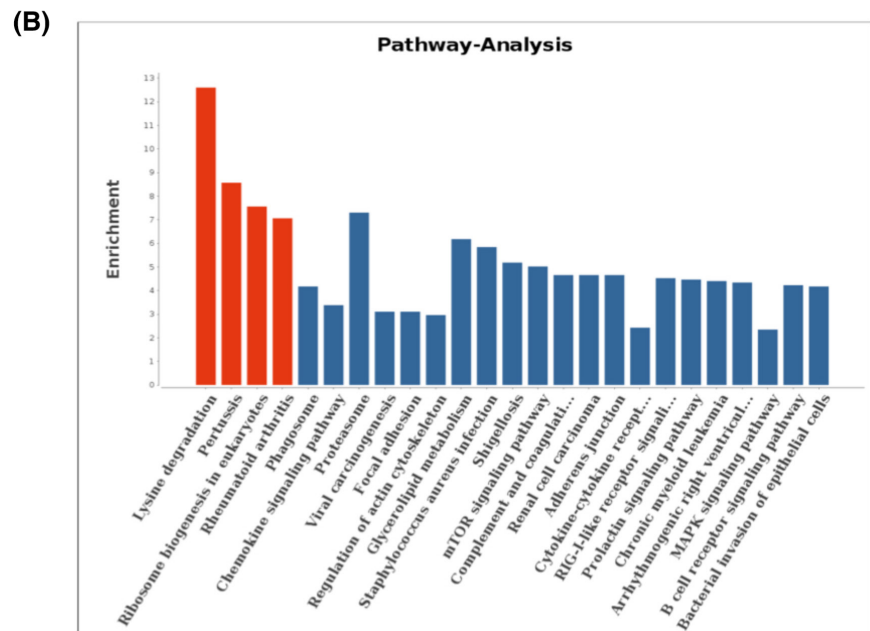
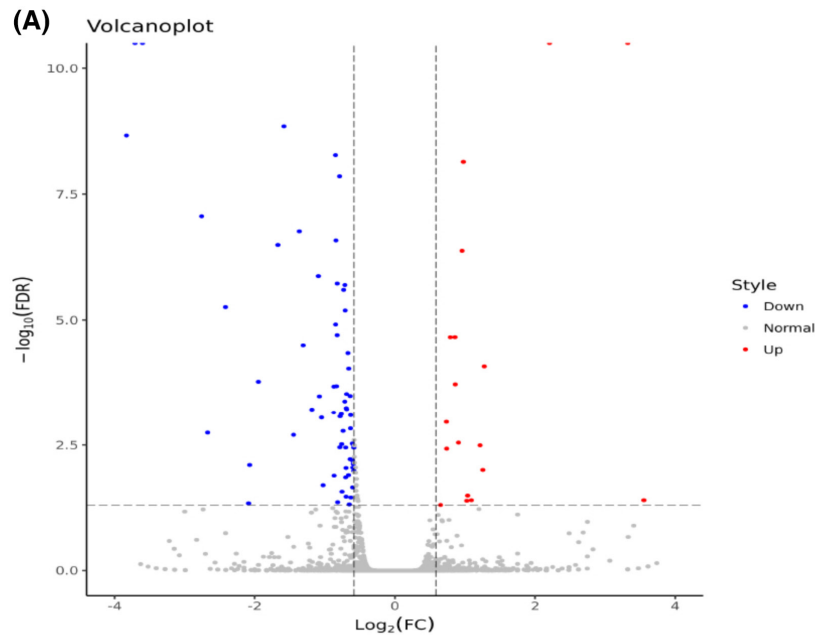
inhibition of autolysosomal degradation steps, resulting in autophagy suppression. To detect whether a treatment induces autophagy, the conversion of LC3B-II into LC3B-I often needs to be determined upon treatment with autophagy inducers in combination with autophagy inhibitors, such as chloroquine (CQ).<sup>31</sup> We first treated cells for 8 h of CQ and then performed the knockdown of circHIPK3. As expected, the conversion of LC3B II-I increased in the si-circ-1/2 and CQ combination groups compared to groups with sole silencing of circHIPK3 or adding CQ (Figure 5B). Histograms show the quantification of band intensities (Figure 5C). The results of electron microscopic analysis showed that circHIPK3 knockdown significantly increased accumulation of autophagic vesicles (more than 3-fold) in hBMSCs (Figure 5D). Immunofluorescence staining analysis of LC3B protein expression showed an upregulation in the circHIPK3 knockdown group and no change in the

control group and HIPK3 knockdown group (Figure 5E). In addition, we established a concentration gradient of autophagy regulator CQ and rapamycin (Rapa) based on several studies.<sup>22,23,25</sup> CircHIPK3 expression was measured after 24 h of treatment with Rapa and CQ. The PCR results showed an obvious upregulation of circHIPK3 after Rapa treatment but no change after CQ treatment (Figure S1A,B).

### 3.6 | Activating autophagy promoted the osteogenesis of hBMSCs while suppressing it inhibited osteogenesis

There are debates on whether autophagy promotes or inhibits the osteogenesis of hBMSCs. We wanted to determine the influence of autophagy on hBMSCs. We used the concentration gradient of autophagy regulator

**FIGURE 4** RNA sequencing results showed the relationship between circHIPK3 and autophagy. (A) The differentially expressed genes in circHIPK3 knockdown group and control group were counted. FDR <0.05 and fold change >1.5 were set as restrictive conditions to identify the differentially expressed genes. (B) KEGG pathway analysis showed the relationship between the differentially expressed genes and different pathways.



CQ and Rapa and increased the concentrations over the course of osteogenic induction. The medium was changed every 3 days. Autophagy activity was measured via western blotting, and the results showed that as the concentration grew higher, the effects of CQ and Rapa grew stronger. CQ caused about a 7-fold increase of LC3B-II/I and a 1.5-fold increase of P62 at 20  $\mu$ m while Rapa caused a 2-fold increase of LC3B-II/I and a 1.5-fold decrease of P62 at 250 nM. The protein level of RUNX2 was also detected (Figure 6A,B). CQ caused a 5-fold reduction of the protein expression of RUNX2 at 20  $\mu$ m while Rapa caused a 1.5-fold increase of RUNX2

at 250 nM. After 3 and 7 days of osteogenic induction, ALP staining and activity were performed and the results proved that activation of autophagy promoted the osteogenesis and vice versa. Overall, the higher the concentration, the stronger the effect on osteogenesis (Figure 6C). Considering the above results, we chose 250 nM of Rapa and 15  $\mu$ M of CQ as the final concentration. ARS staining and quantification after 14 days of osteogenesis showed that stimulating autophagy caused about 2-fold enhancement while inhibiting autophagy produced about a 2-fold decrease of extracellular matrix mineralization of hBMSCs (Figure 6D).

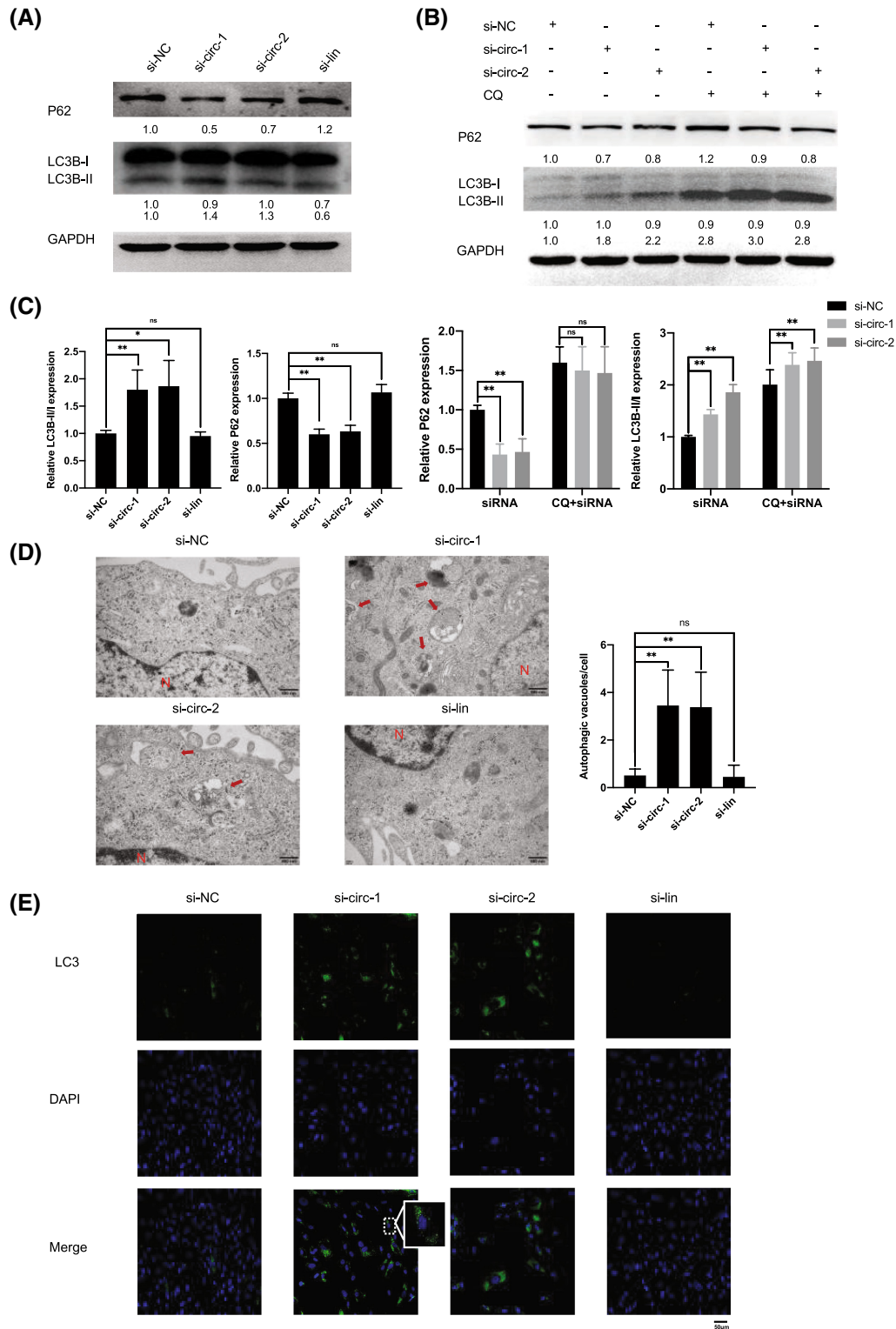


**FIGURE 5** Silencing circHIPK3 activated the autophagy flux. (A) P62 and LC3B expression were measured using western blotting analysis in the si-NC, si-circ-1, si-circ-2, and si-lin groups. (B) CQ was used to treat hBMSCs for 8 h (15  $\mu$ M) and then the transfections were performed. After 72 h of transfection, P62 and LC3B proteins were detected. The intensity of protein band was measured by Image J software and the fold change was listed under each protein band and normalized to GAPDH. (C) Quantification of band intensity was analyzed. (D) The red arrows depicted autophagic vacuoles, and the nucleus was denoted by N. Quantification of autophagic vacuoles was shown in histograms. The number of autophagic vacuoles was determined for a minimum of 20 cells each group. (E) Immunofluorescence staining analysis of LC3B protein expression. The green dots in the white box represent the accumulation of autophagosome (compared to the si-NC group; results are presented as the mean  $\pm$  SD; \* $p < .05$ ; \*\* $p < .01$ ).

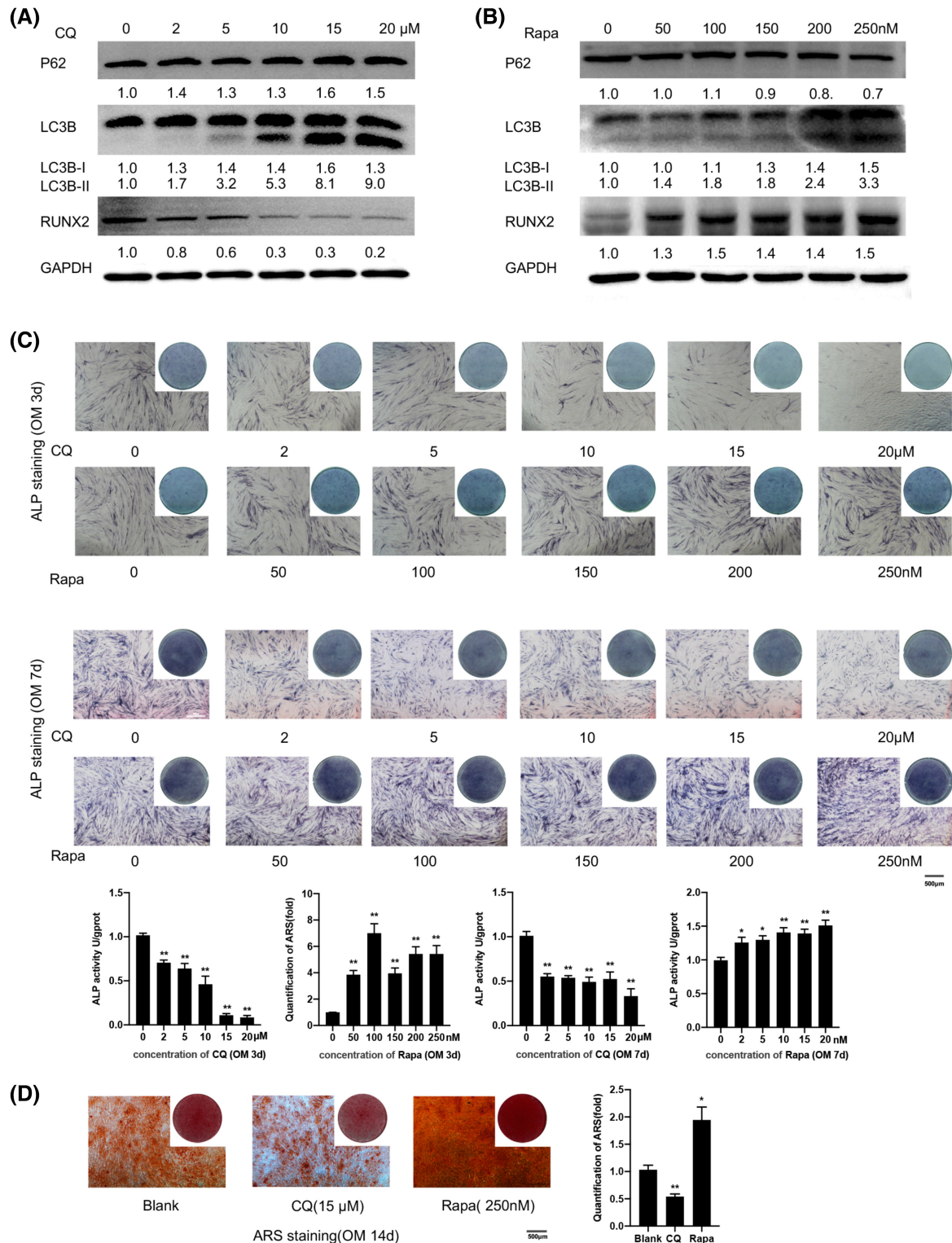


**FIGURE 6** Activation of autophagy promoted the osteogenesis of human BMSCs while suppression of autophagy inhibited osteogenesis. We established a concentration gradient of CQ and Rapa. (A,B) Protein levels of P62, LC3B, and RUNX2 were detected after 24h of treatment with CQ and Rapa. The intensity of protein band was measured by Image J software and the fold change was listed under each protein band and normalized to GAPDH. (C) After 3 and 7 days of osteogenic induction, ALP staining and activity were performed after the constant treatment of CQ and Rapa at different concentrations. (D) ARS staining and quantification were carried out after 14 days of osteogenic differentiation with the treatment of CQ (15 μM) and Rapa (250 nM) (compared to the concentration 0 group and blank group; results are presented as the mean ± SD; \**p* < .05; \*\**p* < .01).

### 3.7 | CircHIPK3 promoted the osteogenic differentiation of hBMSCs by activating autophagy

To determine whether circHIPK3 promoted the osteogenic differentiation of hBMSCs via autophagy regulation, autophagy inhibitor CQ was used. CQ was added into the osteogenic medium at 15  $\mu$ M during the entire osteogenesis. As we predicted, CQ reversed the effects of osteogenesis caused by circHIPK3 knockdown. The RT-PCR results indicated a 3-fold decrease of osteogenic markers ALP and about 2-fold decrease of RUNX2 and OCN after adding CQ (Figure 7A). The RUNX2 protein level was also downregulated after using CQ to inhibit autophagy (Figure 7B). The combination of CQ and siRNAs targeting circHIPK3 caused nearly 5-fold decrease of RUNX2 protein compared to the circHIPK3 knockdown group. ALP staining and activity after 7 days of osteogenesis and ARS staining and quantification after 14 days of osteogenesis showed that CQ compromised the enhanced osteogenesis ability caused by silencing circHIPK3 (Figure 7C,D). The combination of CQ and siRNAs targeting circHIPK3 caused nearly 2-fold decrease of ALP activity and about 3-fold decrease of ARS quantification compared to the circHIPK3 knockdown group.

### 3.8 | CircHIPK3 silencing stimulated autophagy via the release of the binding of HUR to ATG16L1 and upregulated ATG16L1 expression

RNA sequencing results showed that ATG16L1 was upregulated in circHIPK3 knockdown group compared to the control group, which was confirmed to be upregulated thrice by PCR analysis (Figure 8A). Previous studies have shown that HUR can bind to ATG16L1, stabilize its expression, and thus promote autophagy.<sup>42,43</sup> We wondered if circHIPK3 might regulate the expression of ATG16L1 through the release of the binding sites of HUR to ATG16L1. The prediction of the interaction probabilities of circHIPK3 with HUR using bioinformatics was performed, and results indicated that the binding was highly possible (Figure 8B). The protein level of HUR was unchanged after silencing circHIPK3 (Figure 8C). RIP analysis and RNA pull down assay proved that circHIPK3 and ATG16L1 both could bind to HUR, while HIPK3 could not (Figure 8D). RIP analysis showed that RNA expression of ATG16L1 in HUR immunoprecipitation (IP) complex in si-circHIPK3 group was more than twice the expression of si-NC group (Figure 8F). To determine whether the upregulation of ATG16L1 was due to a better stabilization, we performed the mRNA stability assay. We knocked

HUR down using two siRNAs. The silencing efficiency was about 80% and is shown in Figure 8G. The HUR protein was decreased more than 3-fold after knockdown (Figure 8H). We measured ATG16L1 mRNA expression at certain time points by qRT-PCR after treatment with actinomycin D, which stops new RNA synthesis by inhibiting RNA polymerase activity so that the degradation of pre-existing mRNAs could be examined. ATG16L1 degraded faster in the HUR knockdown groups than the control group and degraded more slowly in the circHIPK3 knockdown groups compared to the control group and the HIPK3 knockdown group (Figure 8I). Figure 9 shows that circHIPK3 regulated the osteogenesis via binding to HUR, upregulating ATG16L1 expression and stimulating autophagy.

## 4 | DISCUSSION

CircHIPK3 has an abundant expression in human cells and has been widely studied.<sup>11</sup> Most studies have focused on the relationship of circHIPK3 and cancer.<sup>44</sup> In stem cells, circHIPK3 regulated the differentiation of myoblasts.<sup>45-47</sup> In addition, human umbilical cord MSCs-derived exosomes released circHIPK3 and prevented ischemic injury via the circHIPK3/ FOXO3a axis. Similarly, circHIPK3 from MSC-derived extracellular vesicles inhibited the development of osteoarthritis through the circHIPK3/miR-124-3p/MYH9 pathway.<sup>48</sup> Nevertheless, few studies have investigated the role of circHIPK3 in the osteogenic differentiation of BMSCs. Our work uncovered the negative role of circHIPK3 in the osteogenesis of hBMSCs via initiation of autophagy. Several research studies have uncovered the same phenomenon, where loss of circHIPK3 activates autophagy in a number of cell lines, such as lung cancer cells<sup>14</sup> and colorectal cancer cells.<sup>49</sup> However, some studies have found different results. One study reported that circHIPK3 overexpression activated autophagy and inhibited lipid accumulation in human umbilical vein endothelial cells, demonstrating the role of circHIPK3 in the pathogenesis of atherosclerosis.<sup>50</sup> Moreover, circHIPK3 overexpression has been found to promote the autophagy of cardiomyocytes.<sup>51</sup> These findings, including ours, prove that circHIPK3 plays an important role in autophagy. The regulation of circHIPK3 in autophagy is complicated as it has different effects in different cell lines and circumstances.

As a highly conserved intracellular process, autophagy regulates many biological activities including cancer. Many studies on the potential of autophagy in cancer treatment have been performed.<sup>52</sup> The effects of autophagy on osteogenic differentiation are controversial. However, it is

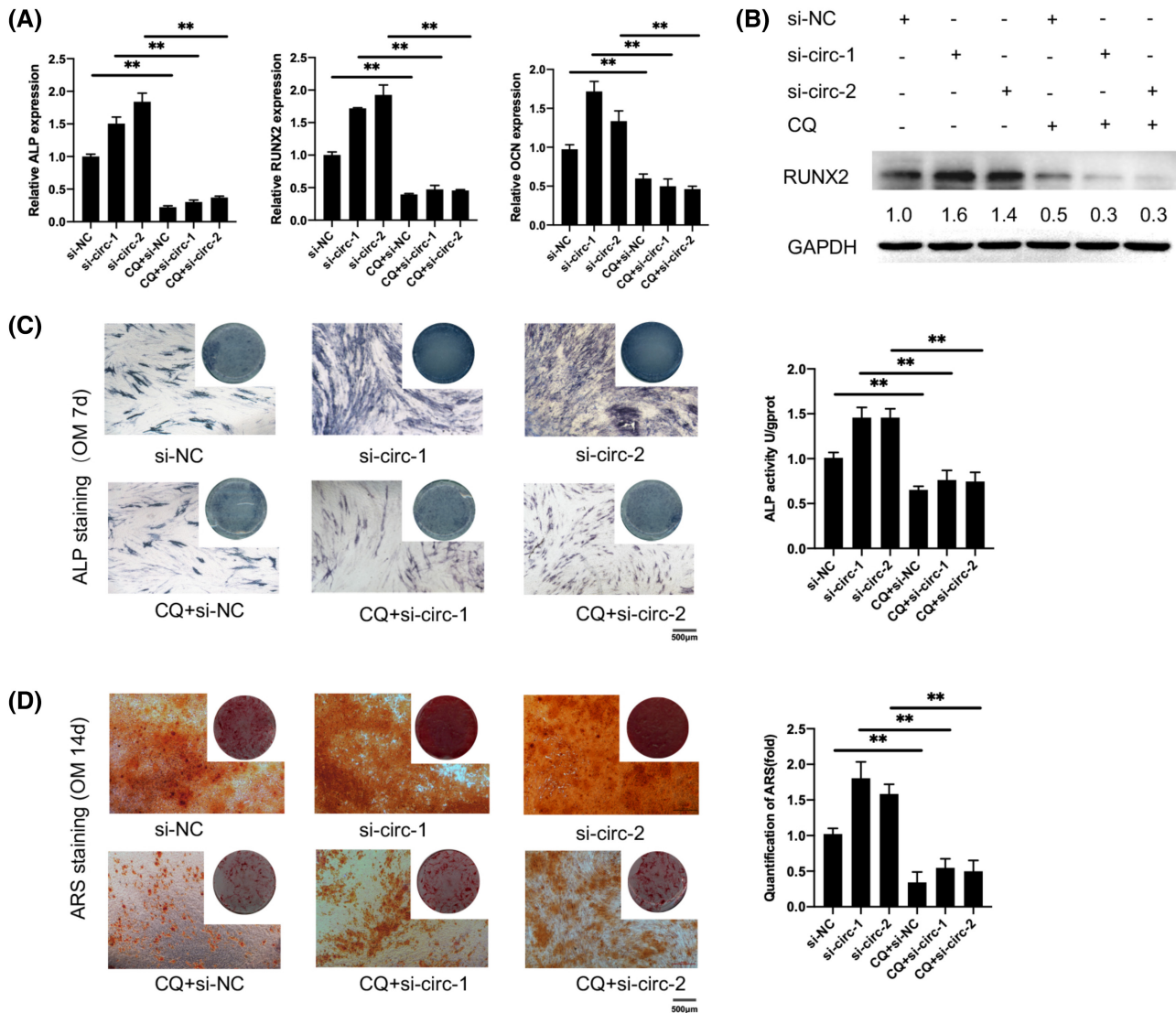


**FIGURE 7** CircHIPK3 promoted the osteogenic differentiation of hBMSCs via activation of autophagy. Osteogenic markers ALP, RUNX2, and OCN (A) and the protein level of RUNX2 (B) were measured after 7 days of osteogenic induction after adding CQ (15  $\mu$ M) in the transfection groups and the control group. ALP staining and activity (C) and ARS staining and quantification (D) were performed after 7 and 14 days of osteogenesis after adding CQ (15  $\mu$ M) (compared to the si-NC group; results are presented as the mean  $\pm$  SD; \* $p$  < .05; \*\* $p$  < .01).

clear that autophagy greatly influences osteogenesis. Our work discovered that activation of autophagy enhanced the osteogenesis while inhibition decreased the osteogenesis of hBMSCs. Because hBMSCs are promising players in the treatment of bone defects, regulating the autophagy level of BMSCs within a moderate range might be a new target for clinical application. Genetic modification, such as modifying circHIPK3 or autophagy regulators, is another option for altering autophagy activity. The translation of basic research on autophagy and osteogenesis into medicine still has a long way to go. The first step should be clarifying the detailed mechanism of how autophagy regulates osteogenesis. In this article, we disclosed the detailed mechanism of circHIPK3 influencing autophagy as a protein sponge. However, how does autophagy affect the

osteogenesis in hBMSCs remains unknown. Further studies are needed on this topic.

HUR is an important regulator of post-transcriptional regulation. In general, it functions via dynamic subcellular localization.<sup>53</sup> It is mainly located in the nucleus, but upon the exposure to stress, it translocates to the cytoplasm.<sup>54</sup> During the translocation process and in the cytoplasm, HUR “guards” the target mRNA and stabilizes it or upregulates its translation. The activation of autophagy caused by serum starvation promotes the cytosolic translocation of HUR.<sup>55</sup> In addition, non-coding RNAs bind to HUR and influence its cytoplasmic translocation. The interaction between circDCUN1D4 and HUR increased the translocation of HUR to the cytoplasm in lung cancer cells.<sup>56</sup> Additionally, a macrophage-specific lncRNA was

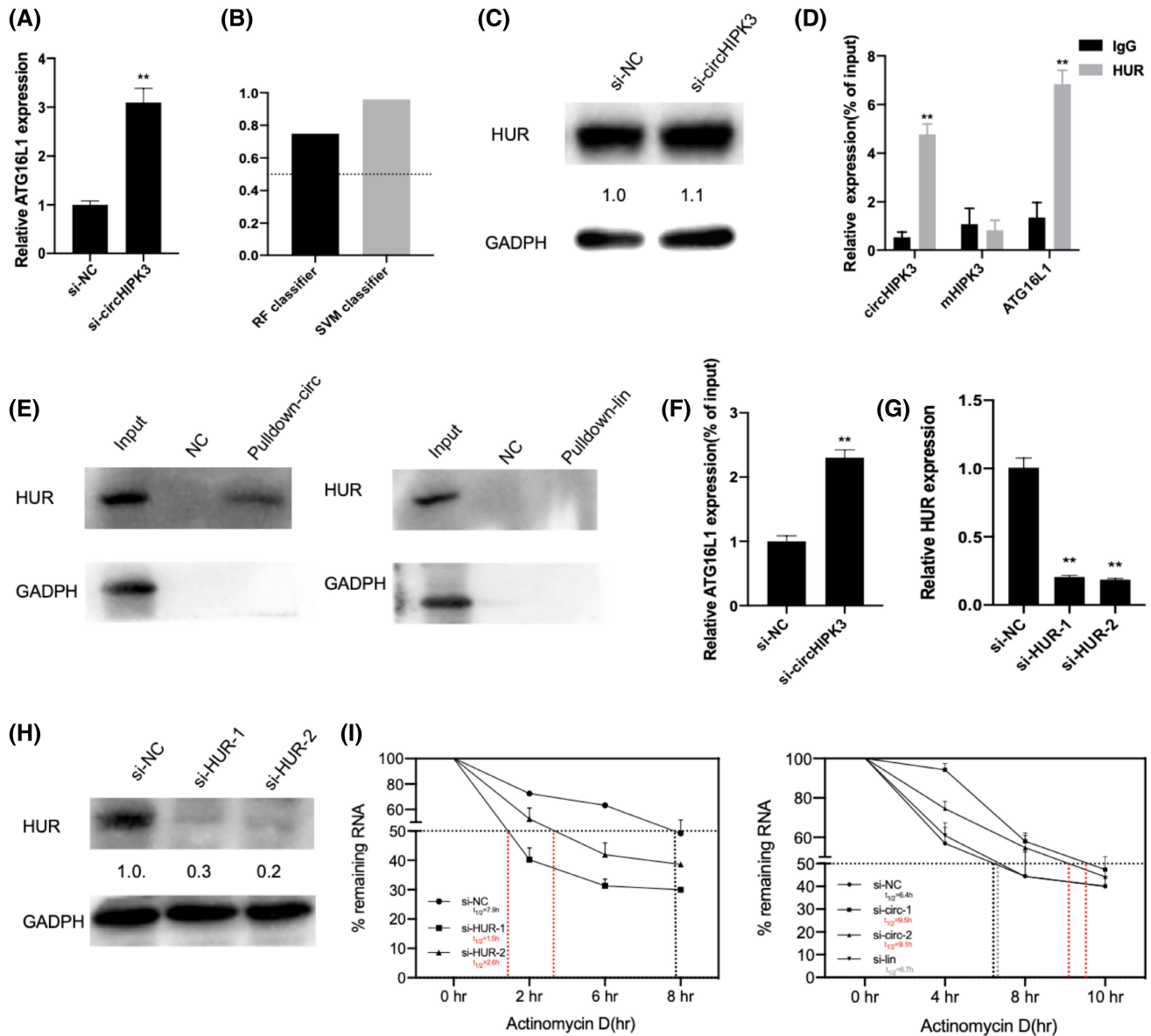


**FIGURE 8** CircHIPK3 silencing stimulated autophagy via releasing the binding of HUR to ATG16L1. (A) qRT-PCR analysis showed the RNA expression of ATG16L1 in the circHIPK3 knockdown group compared to the si-NC group. (B) The prediction of the interaction probabilities of circHIPK3 with RNA binding protein HUR using bioinformatics (<http://pridb.gdcb.iastate.edu/RPISeq/>). Predictions using RF classifier and SVM classifier were considered “positive” when the classifier was  $>0.5$ . (C) The protein expression of HUR was detected in the si-circHIPK3 group compared to the si-NC group. (D) RIP experiments were performed in hBMSCs to detect the binding between HUR and circHIPK3 or mHIPK3 or ATG16L1. The fold enrichment of circHIPK3, mHIPK3, and ATG16L1 in the HUR immunoprecipitation (IP) complex was compared to its matching IgG control, normalized by input. (E) RNA pull down assay was carried out to detect the binding between HUR and circHIPK3 or mHIPK3. (F) RIP was conducted to detect binding between HUR and ATG16L1 after transfection. The RNA expression of ATG16L1 in HUR IP in the si-NC and si-circHIPK3 groups were also detected. (G) HUR was knocked down and the efficiency was measured using qRT-PCR. (H) The protein expression level of HUR after HUR knockdown. (I) ATG16L1 mRNA was measured at certain time points by qRT-PCR after treatment of actinomycin D, which stops new RNA synthesis. The intensity of protein band was measured by Image J software and the fold change was listed under each protein band and normalized to GAPDH (results are presented as the mean  $\pm$  SD; \* $p < .05$ , \*\* $p < .01$ ).

found to bind to HUR and tether it in the nucleus. Based on these results, we had two hypotheses for our work. The first one was that, as silencing circHIPK3 activated autophagy, the stress induced the translocation of HUR and enhanced its guarding effects on ATG16L1. The second

hypothesis was that the interaction between circHIPK3 and HUR influenced the translocated. Our work showed that circHIPK3 was located in both the cytoplasm and nucleus (Figure S1C). Considering the abundant expression of circHIPK3, there should be abundant circHIPK3 in the

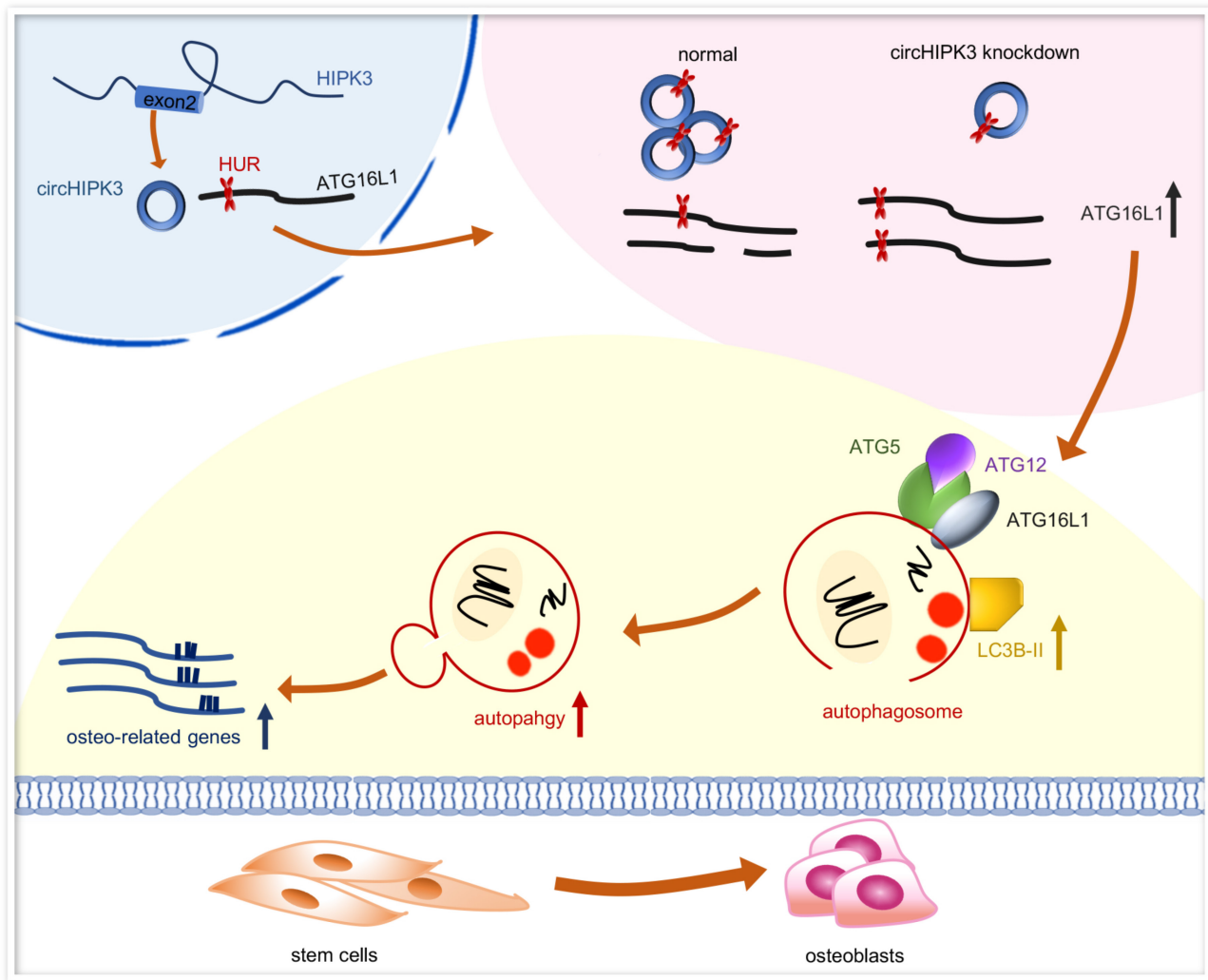


**FIGURE 9** CircHIPK3 regulated osteogenesis. CircHIPK3 is generated from the second exon of HIPK3. Silencing circHIPK3 released the binding sites of HUR to ATG16L1, which resulted in increased binding between HUR and ATG16L1. HUR stabilized the mRNA expression of ATG16L1, and the upregulation of ATG16L1 increased the LC3B lipidation through the interaction of ATG5 and ATG12 to form a large multimeric complex, resulting in the activation of autophagy flux and the promotion of the osteogenesis of hBMSCs.

nucleus, but it is mainly located in the cytoplasm (70%). Thus, it was reasonable to hypothesize that circHIPK3 bound to HUR in the nucleus and affected its translocation. Further work is needed to explore the detailed mechanism. Moreover, HUR has been reported to be involved in autophagy in many different ways. Studies have reported that HUR activates autophagy through stabilization of mRNA of ATG16L1, which is similar to our work. In renal tubular cells, HUR bound to and stabilized LncRNA EGOT expression under normoxia and ATG7/16L1 expressions under hypoxia. EGOT suppressed autophagy by downregulating ATG7, ATG16L1 and LC3B-II expressions.<sup>41</sup> Likewise, HUR regulated ATG7 and ATG16L1 expression and thus mediated autophagy in HK-2 cells.<sup>43</sup> In intestinal epithelial cells, circPABPN1 interacted with HUR as a protein sponge and blocked its combination with ATG16L1 and reduced the positive effects of HUR on

ATG16L1, thereby lowering ATG16L1's production and inhibiting autophagy.<sup>42</sup>

BMSCs have the ability to differentiate into osteoblasts and adipocytes. The balance between osteogenesis and adipogenesis of BMSCs is very important and imbalance could lead to several diseases such as osteoporosis.<sup>57</sup> We have examined the effects of circHIPK3 on the adipogenesis and found that silencing circHIPK3 inhibited the adipogenic differentiation of hBMSCs (Figure S3). Future studies will try to characterize the underlying mechanisms between circHIPK3 and adipogenesis.

To the best of our knowledge, this is the first study to show that the silencing of circHIPK3 facilitates the osteogenic differentiation of hBMSCs via the activation of autophagy flux. Silencing circHIPK3 releases the binding sites of HUR to ATG16L1 and enhances HUR's effects on ATG16L1 by stabilizing mRNA expression. Our research

laid the foundation for further works, which should study how autophagy influences osteogenesis and how to transform the results into possible clinical applications.

## AUTHOR CONTRIBUTIONS

Ziyao Zhuang contributed to conception, design, collection of data, data analysis and interpretation, manuscript draft, and critically revised the manuscript. Chanyuan Jin and Xiaobei Li contributed to collection of data and data analysis. Yineng Han, Qiaolin Yang, and Yiping Huang contributed to data analysis and critically revised the manuscript. Yunfei Zheng and Weiran Li contributed to conception, design, financial support, and critically revised the manuscript. All authors gave final approval and agreed to be accountable for all aspects of the work.

## ACKNOWLEDGMENTS

This study was financially supported by grants from the National Natural Science Foundation of China (Nos. 82071142 and 82071119).

## DISCLOSURES

The author(s) declare that they have no conflict of interest.

## DATA AVAILABILITY STATEMENT

The data that support the findings of this study are available from the corresponding author upon reasonable request.

## ORCID

Ziyao Zhuang  <https://orcid.org/0000-0001-6254-5282>

Chanyuan Jin  <https://orcid.org/0000-0003-0022-5229>

Xiaobei Li  <https://orcid.org/0000-0003-2913-6895>

Yineng Han  <https://orcid.org/0000-0002-8651-3282>

Qiaolin Yang  <https://orcid.org/0000-0003-2987-1881>

Yiping Huang  <https://orcid.org/0000-0003-2263-0612>

Yunfei Zheng  <https://orcid.org/0000-0003-1899-8051>

Weiran Li  <https://orcid.org/0000-0001-9895-1143>

## REFERENCES

- Gomez-Barrena E, Padilla-Eguiluz NG, Avendano-Sola C, et al. A multicentric, open-label, randomized, comparative clinical trial of two different doses of expanded hBM-MSCs plus biomaterial versus iliac crest autograft, for bone healing in non-unions after long bone fractures: study protocol. *Stem Cells Int*. 2018;2018:6025918. doi:10.1155/2018/6025918
- Gomez-Barrena E, Padilla-Eguiluz NG, Garcia-Rey E, et al. Validation of a long bone fracture non-union healing score after treatment with mesenchymal stromal cells combined to biomaterials. *Injury*. 2020;51(suppl 1):S55-S62. doi:10.1016/j.injury.2020.02.030
- Rojewski MT, Lotfi R, Gjerde C, et al. Translation of a standardized manufacturing protocol for mesenchymal stromal cells: a systematic comparison of validation and manufacturing data. *Cytotherapy*. 2019;21(4):468-482. doi:10.1016/j.jcyt.2019.03.001
- Li KC, Chang YH, Yeh CL, Hu YC. Healing of osteoporotic bone defects by baculovirus-engineered bone marrow-derived MSCs expressing MicroRNA sponges. *Biomaterials*. 2016;74:155-166. doi:10.1016/j.biomaterials.2015.09.046
- Hu B, Li Y, Wang M, et al. Functional reconstruction of critical-sized load-bearing bone defects using a sclerostin-targeting miR-210-3p-based construct to enhance osteogenic activity. *Acta Biomater*. 2018;76:275-282. doi:10.1016/j.actbio.2018.06.017
- Memczak S, Jens M, Elefsinioti A, et al. Circular RNAs are a large class of animal RNAs with regulatory potency. *Nature*. 2013;495(7441):333-338. doi:10.1038/nature11928
- Du WW, Yang W, Liu E, Yang Z, Dhaliwal P, Yang BB. Foxo3 circular RNA retards cell cycle progression via forming ternary complexes with p21 and CDK2. *Nucleic Acids Res*. 2016;44(6):2846-2858. doi:10.1093/nar/gkw027
- Ashwal-Fluss R, Meyer M, Pamudurti NR, et al. circRNA biogenesis competes with pre-mRNA splicing. *Mol Cell*. 2014;56(1):55-66. doi:10.1016/j.molcel.2014.08.019
- Yang Y, Fan X, Mao M, et al. Extensive translation of circular RNAs driven by N(6)-methyladenosine. *Cell Res*. 2017;27(5):626-641. doi:10.1038/cr.2017.31
- Zhang M, Zhao K, Xu X, et al. A peptide encoded by circular form of LINC-PINT suppresses oncogenic transcriptional elongation in glioblastoma. *Nat Commun*. 2018;9(1):4475. doi:10.1038/s41467-018-06862-2
- Zheng Q, Bao C, Guo W, et al. Circular RNA profiling reveals an abundant circHIPK3 that regulates cell growth by sponging multiple miRNAs. *Nat Commun*. 2016;7:11215. doi:10.1038/ncomms11215
- Zeng K, Chen X, Xu M, et al. CircHIPK3 promotes colorectal cancer growth and metastasis by sponging miR-7. *Cell Death Dis*. 2018;9(4):417. doi:10.1038/s41419-018-0454-8
- Xiao L, Ma XX, Luo J, et al. Circular RNA CircHIPK3 promotes homeostasis of the intestinal epithelium by reducing MicroRNA 29b function. *Gastroenterology*. 2021;161(4):1303-1317.e3. doi:10.1053/j.gastro.2021.05.060
- Chen X, Mao R, Su W, et al. Circular RNA circHIPK3 modulates autophagy via MIR124-3p-STAT3-PRKAA/AMPKalpha signaling in STK11 mutant lung cancer. *Autophagy*. 2020;16(4):659-671. doi:10.1080/15548627.2019.1634945
- Li Y, Zheng F, Xiao X, et al. CircHIPK3 sponges miR-558 to suppress heparanase expression in bladder cancer cells. *EMBO Rep*. 2017;18(9):1646-1659. doi:10.15252/embr.201643581
- Xie Y, Yuan X, Zhou W, et al. The circular RNA HIPK3 (circHIPK3) and its regulation in cancer progression: review. *Life Sci*. 2020;254:117252. doi:10.1016/j.lfs.2019.117252
- Zheng Y, Li X, Huang Y, Jia L, Li W. The circular RNA landscape of periodontal ligament stem cells during osteogenesis. *J Periodontol*. 2017;88(9):906-914. doi:10.1902/jop.2017.170078
- Mizushima N, Komatsu M. Autophagy: renovation of cells and tissues. *Cell*. 2011;147(4):728-741. doi:10.1016/j.cell.2011.10.026
- Menshikov M, Zubkova E, Stafeev I, Parfyonova Y. Autophagy, mesenchymal stem cell differentiation, and secretion. *Biomedicines*. 2021;9(9):1178. doi:10.3390/biomedicines9091178
- Vidoni C, Ferraresi A, Secomandi E, et al. Autophagy drives osteogenic differentiation of human gingival mesenchymal stem cells. *Cell Commun Signal*. 2019;17(1):98. doi:10.1186/s12964-019-0414-7

21. Yang Y, Lin Z, Cheng J, et al. The roles of autophagy in osteogenic differentiation in rat ligamentum fibroblasts: evidence and possible implications. *FASEB J.* 2020;34(7):8876-8886. doi:10.1096/fj.201903216RR
22. Chen X, Sun K, Zhao S, et al. Irisin promotes osteogenic differentiation of bone marrow mesenchymal stem cells by activating autophagy via the Wnt/ $\beta$ -catenin signal pathway. *Cytokine.* 2020;136:155292. doi:10.1016/j.cyto.2020.155292
23. Zhang P, Zhang H, Lin J, et al. Insulin impedes osteogenesis of BMSCs by inhibiting autophagy and promoting premature senescence via the TGF- $\beta$ 1 pathway. *Aging (Albany NY).* 2020;12(3):2084-2100. doi:10.18632/aging.102723
24. Li Z, Liu X, Zhu Y, et al. Mitochondrial phosphoenolpyruvate carboxykinase regulates osteogenic differentiation by modulating AMPK/ULK1-dependent autophagy. *Stem Cells.* 2019;37(12):1542-1555. doi:10.1002/stem.3091
25. Li N, Yan M, Chen Y, et al. Extracellular IL-37 promotes osteogenic and odontogenic differentiation of human dental pulp stem cells via autophagy. *Exp Cell Res.* 2021;407(1):112780. doi:10.1016/j.yexcr.2021.112780
26. Pieleś O, Hartmann M, Morszczyk C. AMP-activated protein kinase and the down-stream activated process of autophagy regulate the osteogenic differentiation of human dental follicle cells. *Arch Oral Biol.* 2021;122:104951. doi:10.1016/j.archoralbio.2020.104951
27. Gao JW, He WB, Xie CM, et al. Aldosterone enhances high phosphate-induced vascular calcification through inhibition of AMPK-mediated autophagy. *J Cell Mol Med.* 2020;24(23):13648-13659. doi:10.1111/jcmm.15813
28. Chen WR, Yang JQ, Liu F, Shen XQ, Zhou YJ. Melatonin attenuates vascular calcification by activating autophagy via an AMPK/mTOR/ULK1 signaling pathway. *Exp Cell Res.* 2020;389(1):111883. doi:10.1016/j.yexcr.2020.111883
29. Zhang Y, Shen X, Cheng L, et al. Toll-like receptor 4 knockout protects against diabetic-induced imbalance of bone metabolism via autophagic suppression. *Mol Immunol.* 2020;117:12-19. doi:10.1016/j.molimm.2019.10.025
30. Siva Sankar D, Dengjel J. Protein complexes and neighborhoods driving autophagy. *Autophagy.* 2021;17(10):2689-2705. doi:10.1080/15548627.2020.1847461
31. Klionsky DJ, Abdelmohsen K, Abe A, et al. Guidelines for the use and interpretation of assays for monitoring autophagy (3rd edition). *Autophagy.* 2016;12(1):1-222. doi:10.1080/15548627.2015.1100356
32. Hu YP, Jin YP, Wu XS, et al. LncRNA-HGBC stabilized by HuR promotes gallbladder cancer progression by regulating miR-502-3p/SET/AKT axis. *Mol Cancer.* 2019;18(1):167. doi:10.1186/s12943-019-1097-9
33. Chen Y, Yang F, Fang E, et al. Circular RNA circAGO2 drives cancer progression through facilitating HuR-repressed functions of AGO2-miRNA complexes. *Cell Death Differ.* 2019;26(7):1346-1364. doi:10.1038/s41418-018-0220-6
34. Li X, Zheng Y, Zheng Y, et al. Circular RNA CDR1as regulates osteoblastic differentiation of periodontal ligament stem cells via the miR-7/GDF5/SMAD and p38 MAPK signaling pathway. *Stem Cell Res Ther.* 2018;9(1):232. doi:10.1186/s13287-018-0976-0
35. Jin CZ, Jia L, Zheng Y. Long non-coding RNA MIR22HG inhibits the adipogenesis of human bone marrow mesenchymal stem cells with the involvement of Wnt/ $\beta$ -catenin pathway. *Biocell.* 2022;46(7):1717-1724. doi:10.32604/biocell.2022.018706
36. Jin C, Jia L, Huang Y, et al. Inhibition of lncRNA MIR31HG promotes osteogenic differentiation of human adipose-derived stem cells. *Stem Cells.* 2016;34(11):2707-2720. doi:10.1002/stem.2439
37. Jin C, Jia L, Tang Z, Zheng Y. Long non-coding RNA MIR22HG promotes osteogenic differentiation of bone marrow mesenchymal stem cells via PTEN/AKT pathway. *Cell Death Dis.* 2020;11(7):601. doi:10.1038/s41419-020-02813-2
38. Muppírala UK, Honavar VG, Dobbs D. Predicting RNA-protein interactions using only sequence information. *BMC Bioinformatics.* 2011;12:489. doi:10.1186/1471-2105-12-489
39. Dudekula DB, Panda AC, Grammatikakis I, De S, Abdelmohsen K, Gorospe M. CircInteractome: a web tool for exploring circular RNAs and their interacting proteins and microRNAs. *RNA Biol.* 2016;13(1):34-42. doi:10.1080/15476286.2015.1128065
40. Gagliardi M, Matarazzo MR. RIP: RNA immunoprecipitation. *Methods Mol Biol.* 2016;1480:73-86. doi:10.1007/978-1-4939-6380-5\_7
41. Wang IK, Palanisamy K, Sun KT, et al. The functional interplay of lncRNA EGOT and HuR regulates hypoxia-induced autophagy in renal tubular cells. *J Cell Biochem.* 2020;121(11):4522-4534. doi:10.1002/jcb.29669
42. Li XX, Xiao L, Chung HK, et al. Interaction between HuR and circPABPN1 modulates autophagy in the intestinal epithelium by altering ATG16L1 translation. *Mol Cell Biol.* 2020;40(6):e00492-19. doi:10.1128/MCB.00492-19
43. Palanisamy K, Tsai TH, Yu TM, et al. RNA-binding protein, human antigen R regulates hypoxia-induced autophagy by targeting ATG7/ATG16L1 expressions and autophagosome formation. *J Cell Physiol.* 2019;234(5):7448-7458. doi:10.1002/jcp.27502
44. Zhang Y, Liu Q, Liao Q. CircHIPK3: a promising cancer-related circular RNA. *Am J Transl Res.* 2020;12(10):6694-6704.
45. Yao R, Yao Y, Li C, et al. Circ-HIPK3 plays an active role in regulating myoblast differentiation. *Int J Biol Macromol.* 2020;155:1432-1439. doi:10.1016/j.ijbiomac.2019.11.119
46. Gao M, Li X, Yang Z, et al. circHIPK3 regulates proliferation and differentiation of myoblast through the miR-7/TCF12 pathway. *J Cell Physiol.* 2021;236(10):6793-6805. doi:10.1002/jcp.30363
47. Chen B, Yu J, Guo L, et al. Circular RNA circHIPK3 promotes the proliferation and differentiation of chicken myoblast cells by sponging miR-30a-3p. *Cells.* 2019;8(2):177. doi:10.3390/cells8020177
48. Li S, Liu J, Liu S, Jiao W, Wang X. Mesenchymal stem cell-derived extracellular vesicles prevent the development of osteoarthritis via the circHIPK3/miR-124-3p/MYH9 axis. *J Nanobiotechnol.* 2021;19(1):194. doi:10.1186/s12951-021-00940-2
49. Zhang Y, Li C, Liu X, et al. circHIPK3 promotes oxaliplatin-resistance in colorectal cancer through autophagy by sponging miR-637. *EBioMedicine.* 2019;48:277-288. doi:10.1016/j.ebiom.2019.09.051
50. Wei MY, Lv RR, Teng Z. Circular RNA circHIPK3 as a novel circRNA regulator of autophagy and endothelial cell dysfunction in atherosclerosis. *Eur Rev Med Pharmacol Sci.* 2020;24(24):12849-12858. doi:10.26355/eurrev\_202012\_24187
51. Qiu Z, Wang Y, Liu W, et al. CircHIPK3 regulates the autophagy and apoptosis of hypoxia/reoxygenation-stimulated cardiomyocytes via the miR-20b-5p/ATG7 axis. *Cell Death Discov.* 2021;7(1):64. doi:10.1038/s41420-021-00448-6

52. Chen HT, Liu H, Mao MJ, et al. Crosstalk between autophagy and epithelial-mesenchymal transition and its application in cancer therapy. *Mol Cancer*. 2019;18(1):101. doi:10.1186/s12943-019-1030-2
53. Grammatikakis I, Abdelmohsen K, Gorospe M. Posttranslational control of HuR function. *Wiley Interdiscip Rev RNA*. 2017;8(1):e1372. doi:10.1002/wrna.1372
54. Nabors LB, Gillespie GY, Harkins L, King PH. HuR, a RNA stability factor, is expressed in malignant brain tumors and binds to adenine- and uridine-rich elements within the 3' untranslated regions of cytokine and angiogenic factor mRNAs. *Cancer Res*. 2001;61(5):2154-2161.
55. De S, Das S, Sengupta S. Involvement of HuR in the serum starvation induced autophagy through regulation of Beclin1 in breast cancer cell-line, MCF-7. *Cell Signal*. 2019;61:78-85. doi:10.1016/j.cellsig.2019.05.008
56. Liang Y, Wang H, Chen B, et al. circDCUN1D4 suppresses tumor metastasis and glycolysis in lung adenocarcinoma by stabilizing TXNIP expression. *Mol Ther Nucleic Acids*. 2021;23:355-368. doi:10.1016/j.omtn.2020.11.012
57. Zhi F, Ding Y, Wang R, Yang Y, Luo K, Hua F. Exosomal hsa\_circ\_0006859 is a potential biomarker for postmenopausal

osteoporosis and enhances adipogenic versus osteogenic differentiation in human bone marrow mesenchymal stem cells by sponging miR-431-5p. *Stem Cell Res Ther*. 2021;12(1):157. doi:10.1186/s13287-021-02214-y

## SUPPORTING INFORMATION

Additional supporting information can be found online in the Supporting Information section at the end of this article.

**How to cite this article:** Zhuang Z, Jin C, Li X, et al. Knockdown of circHIPK3 promotes the osteogenic differentiation of human bone marrow mesenchymal stem cells through activating the autophagy flux. *The FASEB Journal*. 2022;36:e22590. doi:10.1096/fj.202200832R